ChemSusChem

Research Article
doi.org/10.1002/cssc.202301903

Chemistry Europe
European Chemical Societies Publishing

www.chemsuschem.org

Ferrocene Appended Porphyrin-Based Bipolar Electrode Material for High-Performance Energy Storage

Shagor Chowdhury,*[a, b] Saibal Jana,[a] Sai. P. K. Panguluri,[c] Wolfgang Wenzel,[a] Svetlana Klayatskaya,*[a] and Mario Ruben*[a, b, c]

The versatile properties of bipolar organic electrode materials have attracted considerable attention in the field of electrochemical energy storage (EES). However, their practical application is hindered by their inherent limitations including low intrinsic electrical conductivity, low specific capacity, and high solubility. Herein, a bipolar organic molecule combining both porphyrin and ferrocene moieties (CuDEFcP) [5,15-bis(ethynyl)-10,20-di ferrocenyl porphinato]copper(II)) has been developed. It is proposed as a new organic electrode material with multifunctional application for rechargeable organic lithium-based batteries (ROLBs) and dual-ion organic symmetric batteries (SDIBs). Superior performance was delivered as cathode material in lithium based dual-ion batteries (LDIBs), with a high initial discharge capacity of 300 mAh.g^{-1} at 0.2 A.g^{-1} and a reversible capacity of 58 mAh.g^{-1} after 5000 cycles at 1 A.g^{-1}. However, employing it as an anode material in lithium-ion batteries (LIBs), a reversible capacity of 295 mAh.g^{-1} at 0.2 A.g^{-1} was delivered. In SDIBs, in which CuDEFcP is used as both anode and cathode, an average discharge voltage of 2.4 V and an energy density of 261 Wh.kg^{-1} were achieved.

Introduction

The rapid depletion of fossil fuels and the escalating environmental crisis have led to a strong emphasis on the transition toward renewable and sustainable energy sources.[1] As a response, it requests the development of electrical energy storage devices with higher standards that can be integrated into smart electrical grids.[2] Out of the different energy storage devices available, rechargeable batteries are considered as one of the most efficient technologies for storing electrical energy. For decades, rechargeable lithium-ion batteries (LIBs) have been commercialized and they play a vital role as the primary power source in mobile electronics and electric vehicles.[3] However, the major concern relies on the limited and uneven distribution of lithium resources along with the pollution imposed upon its utilization with conventional inorganic electrode materials.[4] In this prospect, organic materials are considered fascinating alternatives due to their lower CO_2 footprint, ample availability in terms of resources, convenient recyclability and favourable disposal methods. Moreover, their structure can be tailored by moderate synthetic methods, enabling the adjustment and optimization of their properties as well the development of new types of organic electrode materials.[5]

In general, organic electrode materials are classified into three categories: i) n-type materials, are initially reduced to form a negatively charged state, allowing them to attract positively charged cations (such as Li^+, Na^+, or K^+).[6] ii) p-type materials, which are oxidized first to form a positively charged state, enabling them to attract negatively charged anions (like PF_6^-, $TFSI^-$, or ClO_4^-).[7] iii) Bipolar-type organic compounds possess characteristics of both n-type and p-type materials.

Porphyrin and its derivatives feature bipolar type properties where their flat conjugated aromatic macrocyclic structure with 18 π-electrons are capable of undergoing multiple electron transfers, either by oxidation into 16 π-electrons or by reduction into 20 π-electrons.[8] Furthermore, they possess fast redox kinetics due to their small highest occupied molecular orbital (HOMO) and lowest unoccupied molecular orbital (LUMO) gaps.[9] Over the past few years, there has been a growing interest in utilizing porphyrin compounds as electrode materials in rechargeable batteries. For instance, Wu and co-authors showcased tetrakis(4-carboxyphenyl) porphyrin (TCPP) as an anode, achieving notable result with high specific reversible capacity (1200 mAh.g^{-1}) and excellent rate capability.[10] Shin and co-authors reported the application of dimesityl-substituted norcorrole nickel(ii) complex (NiNC) as both cathode and anode revealing an initial discharge capacity of 86 mAh.g^{-1} in a Li-metal-free battery.[11] However, similar to many other organic compounds, porphyrins suffer from significant dissolution issues in aprotic electrolytes. This results in rapid capacity decay and

[a] S. Chowdhury, S. Jana, W. Wenzel, S. Klayatskaya, M. Ruben
Institute of Nanotechnology (INT), Karlsruhe Institute of Technology (KIT), Eggenstein-Leopoldshafen D-76344, Germany
E-mail: schowdhury@unistra.fr
svetlana.klyatskaya@kit.edu
mario.ruben@kit.edu

[b] S. Chowdhury, M. Ruben
Centre Européen de Sciences Quantiques (CESQ), Institut de Science et d'Ingénierie Suparamolaiculaires (ISIS), Strasbourg Cedex F-67083, France

[c] S. P. K. Panguluri, M. Ruben
Institute for Quantum Materials and Technology (IQMT), Karlsruhe Institute of Technology (KIT), Eggenstein Leopoldshafen D-76344, Germany

Supporting information for this article is available on the WWW under https://doi.org/10.1002/cssc.202301903

poor cycling stability. To counter this issue, different strategies have been implemented. One of the approaches relies in the polymerization of the porphyrin beforehand chemically or electrochemically,[12] and the other involves the *in-situ* electrochemical polymerization during the cycling process.[13] In this perspective, [5,15-bis(ethynyl)-10,20-diphenylporphinato] copper(II) (CuDEPP) was reported as a self-conditioned electrode material for lithium-ion batteries, exhibiting excellent electrochemical performance.[14] The versatile nature of the ethynyl group introduced at the *meso*-position of the porphyrin has been shown to enhance the electrode's structural stability and conductivity.

From previous investigations, it has been learned that the introduction of suitable redox-active functional units into porphyrin macrocycle results in a multiple electron transfer and hence improves the specific capacity.[15] Moreover, the existence of electronic communication in *meso*-substituted porphyrins with ferrocene has been demonstrated in which the central iron (II) cation (Fe^{2+}) and two cyclopentadienyl anions could perform reversible redox reactions, where Fe^{2+} in ferrocene could be oxidized into Fe^{3+}.[16] Therefore we envisioned that porphyrins bearing ferrocene substituent can be utilized as promising organic electrode material. Accordingly, the electrochemical performances of four different ferrocene functionalized porphyrins have been screened (**H_2FcPh_3P** – [$FcPh_3P$ = 5-ferrocenyl-10,15,20-triphenyl porphyrin(2−)], **H_2TFcP** – [TFcP = 5,10,15,20-tetraferrocenyl porphyrin(2−)], **CuTFcP** – [5,10,15,20-tetra(ferrocenyl)porphyrin] Copper(II) and **CuDEFcP** – [5,15-bis(ethynyl)-10,20-di ferrocenyl porphinato]copper(II)) as potential electrode materials for rechargeable organic lithium-based batteries (ROLBs) (Figure 1).

Results and Discussion

The development of stable organic cathode materials for rechargeable batteries with high theoretical capacity has always captured broad attention. To maximize the capacity, we incorporated multiple redox active ferrocene units with the porphyrin. Four porphyrins **H_2FcPh_3P**, **H_2TFcP**, **CuTFcP**, and **CuDEFcP** have been synthesized (Figures S1-S23) and screened as a cathode material in lithium based dual-ion batteries (LDIBs) within the voltage range of 1.8–4.5 V (Figure S24). The results recorded from the cyclic performances of H_2FcPh_3P, H_2TFcP, and CuTFcP fell significantly short of the anticipated theoretical capacity. However, CuDEFcP displayed optimal cycling performance with high specific capacity compared with the other counterparts. To better understand it's the charge storage capability and reversibility, density functional theory (DFT) simulation has been performed.

From theoretical point of view, lower HOMO-LUMO gap (ΔE) facilitates the transfer of electrons and hence enhances the rate stability.[17] CuDEFcP exhibited a lower HOMO-LUMO gap (2.43 eV) compared to CuTFcP (2.52 eV) and H_2FcPh_3P (2.59 eV), and a slightly higher one compared to H_2TFcP (2.40 eV), endowing it with good electronic conductivity and fast redox kinetics (Figure S25). Moreover, in the oxidized and reduced state, the HOMO-LUMO gap of CuDEFcP was found to be 1.28 eV and 1.03 eV, respectively (Figure S26), indicating that CuDEFcP is stable in all the redox states.[18]

As planarity plays a crucial role in charge storage process,[19] the geometries of the different porphyrin derivatives have been further analyzed in the presence and absence of PF_6^-. For H_2FcPh_3P, the planar porphyrin core was found distorted upon the introduction of two PF_6^- ions, that might result in a low storage capacity. In the case of H_2TFcP, the incorporation of three additional ferrocene moieties led to a significant loss of planarity too. Consequently, the presence of two PF_6^- ions caused more pronounced structural deformation, indicating to a reduced storage capability. Similar outcome has been found with CuTFcP despite the presence of copper metal that might mitigate the planarity disruption and render its rigidity. Once more, when two ethynyl groups and two ferrocene moieties were present (CuDEFcP), the planarity of the geometry was also disrupted. Remarkably, the geometry remained largely undisturbed in the presence of two and four PF_6^- ions, highlighting its superior storage capacity compared to other porphyrin derivatives examined in this study (Figures S27 and S28).

The above results along with the low molecular weight renders CuDEFcP as a suitable cathode material with an increased reversible capacity. From the structural point of view, the ethynyl units can maximize the π-π stacking interaction within molecules,[20] and its presence in CuDEFcP has been found to reduce the solubility of the active material within the electrolyte (Figure S29). Based on these outcomes, CuDEFcP was chosen as a model material and further thoroughly

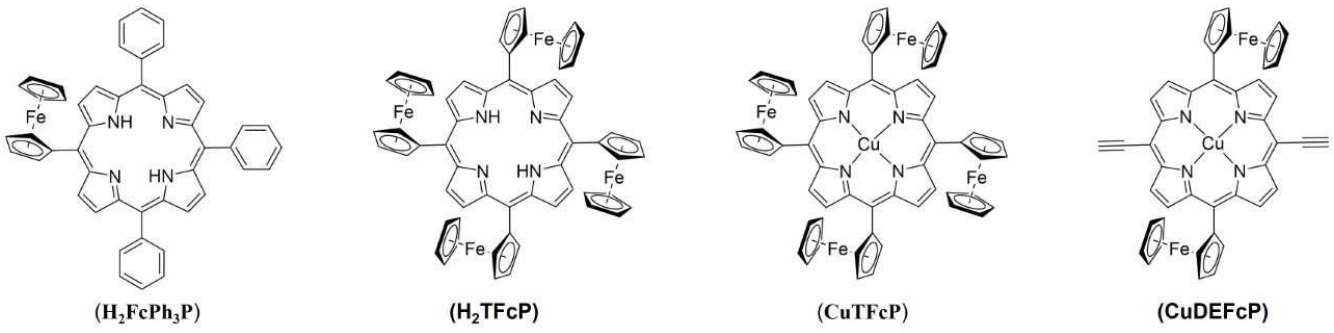

Figure 1. Chemical structures of the four screened ferrocene functionalized porphyrins.

investigated its redox properties for electrochemical energy storage (EES).

CuDEFcP as Cathode Material in LDIBs

The redox property of CuDEFcP has been assessed as a cathode material by means of cyclic voltammetry (CV) within the potential range of 1.8–4.5 V (*vs* Li^+/Li) at scan rate of 0.1 mV.s^{-1}. Herein, CuDEFcP has been employed as a working electrode and Li-foil as a counter electrode.

During the first anodic sweep (Figure 2a), two anodic peaks appeared that might be ascribed to the oxidation of CuDEFcP into cationic species $[CuDEFcP]^{4+}$ and the peak located at 3.51 V is mostly associated with the oxidation of ferrocene units into ferrocenium.[16d,21] The observed irreversible process is a common feature for this class of compounds and will be discussed further later.[14a,15a,22] In the reverse scan, four cathodic peaks were observed. The peaks at 3.41 V and 2.93 V are attributed to the reduction of $[CuDEFcP]^{4+}$ to $[CuDEFcP]^{2+}$ and $[CuDEFcP]^{2+}$ to $[CuDEFcP]^{0}$, respectively. Similarly, the peaks at 2.47 V and 2.25 V are attributed to the reduction of [CuDEFcP] to $[CuDEFcP]^{2-}$ and $[CuDEFcP]^{2-}$ to $[CuDEFcP]^{4-}$, respectively (Figure S30). In the subsequent cycles ($2^{nd}\rightarrow10^{th}$), the irreversible oxidation wave disappears. The peaks located at 4.34 V, 2.47 V and 2.25 V are gradually attenuated, while the peaks at 3.41 V, 2.93 V merged to form a broad reversible redox couple ($\approx$3.2/3.1 V) similar to that of pseudocapacitor which might be caused by the fast electrochemical process.[23] From cycles ($10^{th}\rightarrow20^{th}$), highly reversible CVs were recorded with a slight shift to lower potential (Figure 2a). This behaviour accounts for the increase in electrical conductivity of the material upon cycling,[24] which has been further verified by electrochemical impedance spectroscopy (EIS), in which the charge-transfer resistance of the CuDEFcP electrode has reduced after the initial cycle (Figure S31).

Galvanostatic charge/discharge (GCD) was applied to further evaluate the electrochemical properties of CuDEFcP electrode within the potential range of 1.8–4.5 V. During the first cycle, an irreversible charge/discharge process was observed. CuDEFcP delivered a charged capacity of 837 mAh.g^{-1} with the appearance of a voltage plateau around 3.5 and 4.4 V and a discharged capacity of 300 mAh.g^{-1} (Figure 2b). In line with the CV experiment, the high irreversible process was observed only during the first cycle. In the following cycles, in particular from the third cycle, more reversible charge/discharge processes were observed with the absence of a well-defined horizontal voltage plateau, signifying to a rapid multiple pseudo-capacitive redox reaction.[25] The capacity contribution of carbon black is negligible (Figure S32). During the third cycle, a discharge

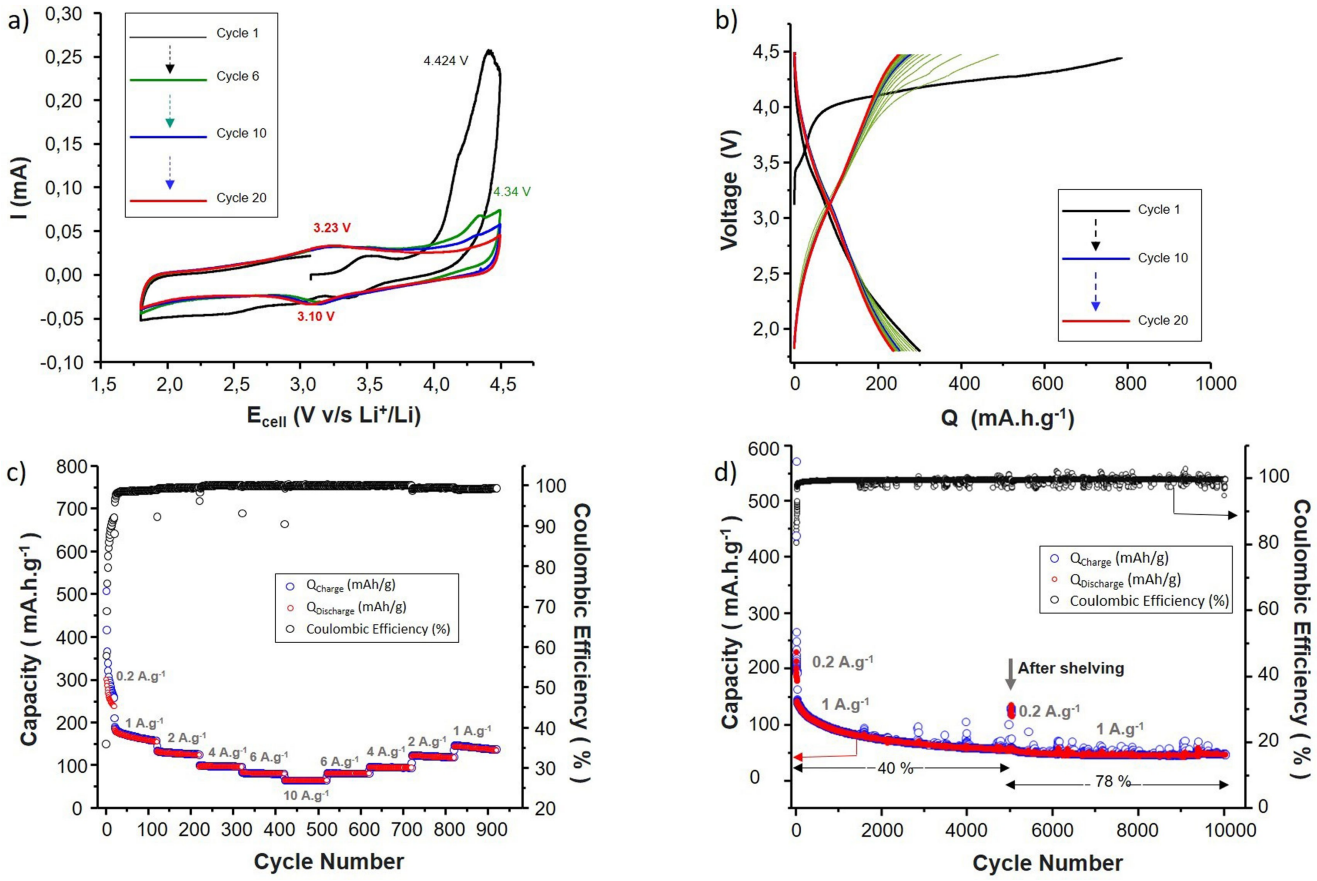

Figure 2. [SC1]
(a) Selected CVs in the range of 4.5–1.8 V at a scan rate of 0.1 mV.s^{-1}. (b) Charge and discharge profiles at 200 mA.g^{-1}.(c) Rate capability.(d) Cycling performance of CuDEFcP cathode.

capacity of 277 mAh.g^{-1} was recorded which is close to the theoretical value of 272 mAh.g^{-1}, and correlated to the eight-electron transfer reaction. The specific discharge capacity then slightly decreased until the tenth cycle and stabilized at 253 mAh.g^{-1} (based on the mass of active material) with an average discharge voltage of 2.8 V at a current density of 200 mA.g^{-1}. This corresponds to a specific energy density of 700 Wh.kg^{-1} and specific power of 360 W.kg^{-1}. The presence of multiple electron transfer has been confirmed by the presence of several subtle weak potential peaks in the dQ/dV curves during the discharge process (Figure S33). In general, the ferrocene within CuDEFcP is expected to contribute in two electron transfer and the porphyrin in 4 electron transfer processes.[13a,14a] However, the existence of multiple Li ion insertion within porphyrin in a potential below 3 V have been previously reported by Cui and coworkers.[10] Recently, Gao and coworkers have reported the 8e$^-$ process in thiophene substituted porphyrin and demonstrated that Li ions interact directly with nitrogen atoms of the porphyrin.[15b] This indicates that Li ions have a main enrollment for the electrochemical process in a potential range below 3 V versus Li$^+$/Li. Therefore, we hypothesized the additional capacity observed in CuDEFcP could originate from multiple lithiation/delithiation reaction in a porphyrin ring. To check the former mentioned feasibility of multiple Li ion insertion within porphyrin ring, electrochemical measurement has been conducted in wider potential window (Figure S34). The CV recorded within a potential range 1–4.5 V, displayed additional reductive peak around 1.7 V in the initial cycle indicating that a redox reaction happened between 1–1.8 V. The galvanostatic charge discharge recorded within the same potential range (1–4.5 V) resulted in a higher charge discharge capacity. These results suggest that the porphyrin ring in CuDEFcP has the potential to store additional lithium ions.

The rate performance of CuDEFcP was tested at different current densities ranging from 0.2 A.g^{-1} to 10 A.g^{-1}. As shown in Figure 2c, CuDEFcP delivered discharge capacities of 185, 133, 99, and 83 mAh.g^{-1} at current densities 1, 2, 4, and 6 A.g^{-1}, respectively within 100 cycles. At high current density of 10 A.g^{-1} (Figure S35) the material was capable of delivering a discharge capacity of 65 mAh.g^{-1} within 36 s with a coulombic efficiency around 100%. These values correspond to a specific energy density of 177 Wh.Kg^{-1} and specific power of 18 kW.Kg^{-1}. Remarkably after the back-and-forth deep cycling, most of the discharge capacity is recovered when the current density is returned back to 1 A.g^{-1}. This demonstrates an excellent rate capability feature of the material as a cathode electrode. The long-term cycling performance was evaluated at 1 A.g^{-1} after it was initially cycled at 0.2 A.g^{-1} for 20 cycles (Figures 2d). The electrode displayed a reversible capacity of 145 mAh.g^{-1} and it maintained a capacity of 58 mAh.g^{-1} after 5000 cycles, corresponding to a capacity retention of 40%. Later, the cell was stored for 1 month, then it was cycled again at a current density of 0.2 A.g^{-1} for 20 cycles followed by cycling at 1 A.g^{-1} for additional 5000 cycles. The material was able to deliver a reversible specific capacity of 45 mAh.g^{-1} with a capacity retention 78% within the next 5000 cycles. Taken all together, CuDEFcP showed a stable cycling performance as a cathode material (10,000 cycles in total) with a fast charge-discharge capability.

To gain information on the electrochemical kinetics of CuDEFcP electrode, CVs at different scan-rate were performed. This study allows to differentiate between diffusion and capacitive controlled redox processes. The relationship between the measured peak current (i) and scan rate (v) in CV curves can be written as:[23] $I = av^b$, in which a and b are adjustable parameters. A b value of 0.5 indicates a dominant diffusion-controlled behaviour, while a b value of 1 suggests a dominant capacitive behaviour. Therefore, the plot of log (i) versus log (v) allows to calculate the b value from the slope. Herein, the b values were calculated to be 0.82–0.89 (Figures 3a,b). This suggests that the kinetic of charge storage is a mixture of process dominated by capacitive effect. The contribution ratios from the diffusion and capacitive behaviour has been further determined by using the following method:[26] $I_{tot}(V) = k_1\nu + k_2\nu^{1/2}$, where $k_1\nu$ and $k_2\nu^{1/2}$ correspond to the capacitive effects and to the diffusion-controlled effect, respectively. Regarding CuDEFcP, the pseudocapacitive contribution increased from 45% to 78% upon increasing the scan rate from 0.1 mV.s^{-1} to 2 mV.s^{-1} (Figures 3c). It suggests that charge storage is

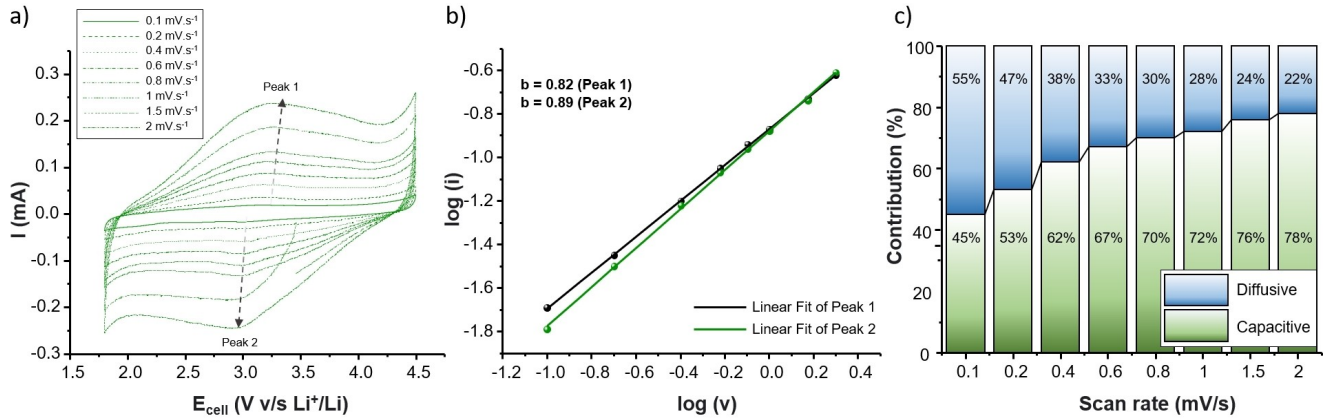

Figure 3. (a) CV curves at different scan rates. (b) plots log(i) versus log(v) at each redox peak, and (c) contribution ratio of pseudocapacitive at various scan rates.

dominated by capacitive process especially at high scan rates, and also supports the fast charge-transfer kinetics between the electrolyte and the electrode.

It is worth to mention that modifying the substituents in the *meso*-position of the porphyrin or removing the metal showed significant influence toward the charge storage contributions. For instance, substituting the acetylene units by ferrocene moieties as in the case of CuTFcP led to a dominant contribution of diffusion-controlled faradaic process. Whereas, removing the metal as in the case of H_2TFcP led to a dominant contribution of capacitive process (Figure S36).

Post Mortem Analysis

The aim of these experiments was to verify the reversible ion-association/dissociation during the charging and discharging process and to identify the reasons leading to the irreversible process observed during the initial cycle. Therefore, *ex-situ* scanning electron microscopy (SEM) measurements combined with energy dispersive X-ray (EDX) and infra-red (IR) analyses have been performed on both charged (4.5 V *vs* Li^+/Li) and discharged (1.8 V *vs* Li^+/Li) electrodes after being carefully rinsed with propylene carbonate (PC) and dimethyl carbonate (DMC).

In general, CuDEFcP could be oxidized into a cationic species upon charging and could be reduced into neutral and/or anionic species upon discharging. Therefore, it could be seen that during the charge process Li^+ is drawn toward the anode and PF_6^- is captured by the cationic species into the electrode from the electrolyte. Whereas during the discharge process, PF_6^- could be released back into the electrolyte where they react with the released Li^+ from the anode to form $LiPF_6$ (Figure 4).[27]

As a control experiment, SEM/EDX spectra and the corresponding elemental mapping of the electrode in the pristine state showed the absence of Phosphorous (P) element while significant amounts of Fluorine (F) element were present resulted from the use of Polyvinylidene Fluoride (PVDF) as a binder (Figure S37). The charged electrode (4.5 V *vs* Li^+/Li) resulted in the increase of P and F percentages, indicating that the PF_6^- is captured by the charged CuDEFcP electrode (Figure 5 and Figure S38). In contrast, the discharged electrode (1.8 V *vs* Li^+/Li) showed a decrease in the percentages of P and F, indicating that the PF_6^- is released back into the electrolyte (Figure 5 and Figure S38). Then recharging the electrode resulted in the increase P and F percentages again, indicating the recapturing of the PF_6^- by CuDEFcP (Figure 5 and Figure S38). Moreover, *ex-situ* IR spectroscopy confirmed the insertion and removal of PF_6^- ions in the electrode (Figure S39). After the cell was charged, signals corresponding to PF_6^- at 838 cm^{-1} and 556 cm^{-1} were detected. Conversely in the discharged state, these signals were obscure.

Insights into the binding sites of the active material (CuDEFcP) with anions/cations (Li^+/PF_6^-) have been obtained from the electrostatic potential (ESP) distributions analysis (Figure 6a).[28] The sites with more negative ESP (blue) are more favorable for Li^+ attraction, while the sites with more positive ESP (red) are more favorable for PF_6^- attraction.[29] In the discharged state, the region surrounding the N atom of the porphyrin ring displayed more negative ESP value, indicating a high affinity for combining with Li^+ ions. In contrast, the porphyrin ring and one of the cyclopentadienyls displayed high ESP values, an indication of being the active sites for PF_6^- binding. Analysis of the optimized structures of ($CuDEFcP^{4+} + 4Li^+$) and ($CuDEFcP^{4+} + 4\ PF_6^-$) have revealed that the lithium ions are located close to the nitrogens and are distributed above and below the ring, whereas the PF_6^- ions are distributed in a region close to the cyclopentadienyls above and below the porphyrin core (Figure 6b and Figure S40).

Experimental evidences for the charge storage mechanism were obtained from *ex-situ* IR spectra recorded for the cycled electrodes. Upon charging, the absorption signal corresponding to the metal ring (Ferrocene) stretching vibration located at

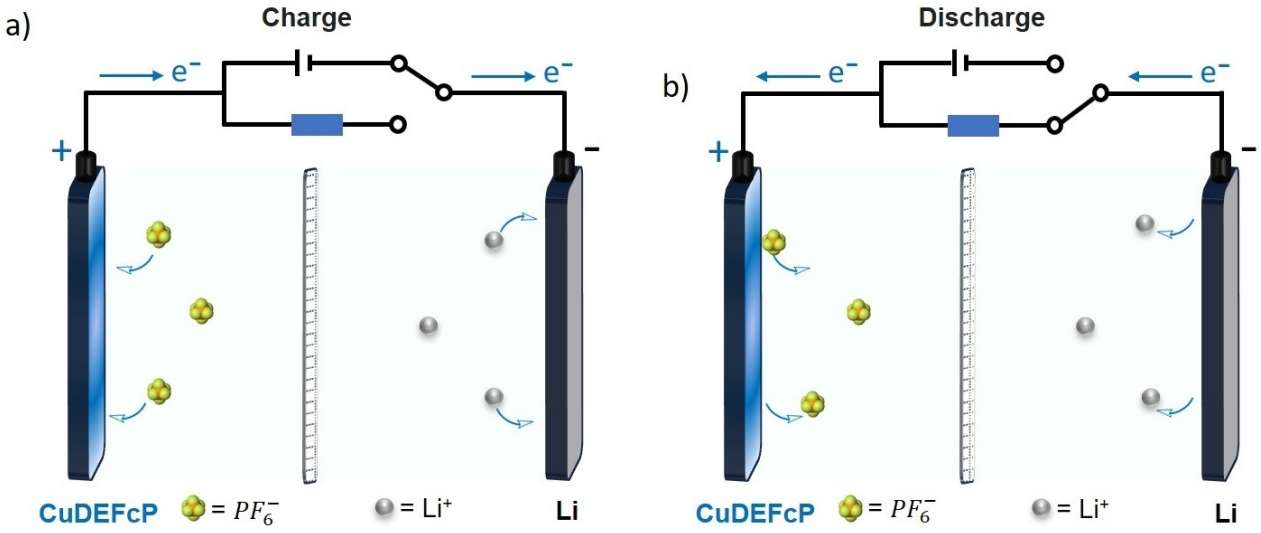

Figure 4. Schematic presentation of possible electrochemical reaction mechanisms.

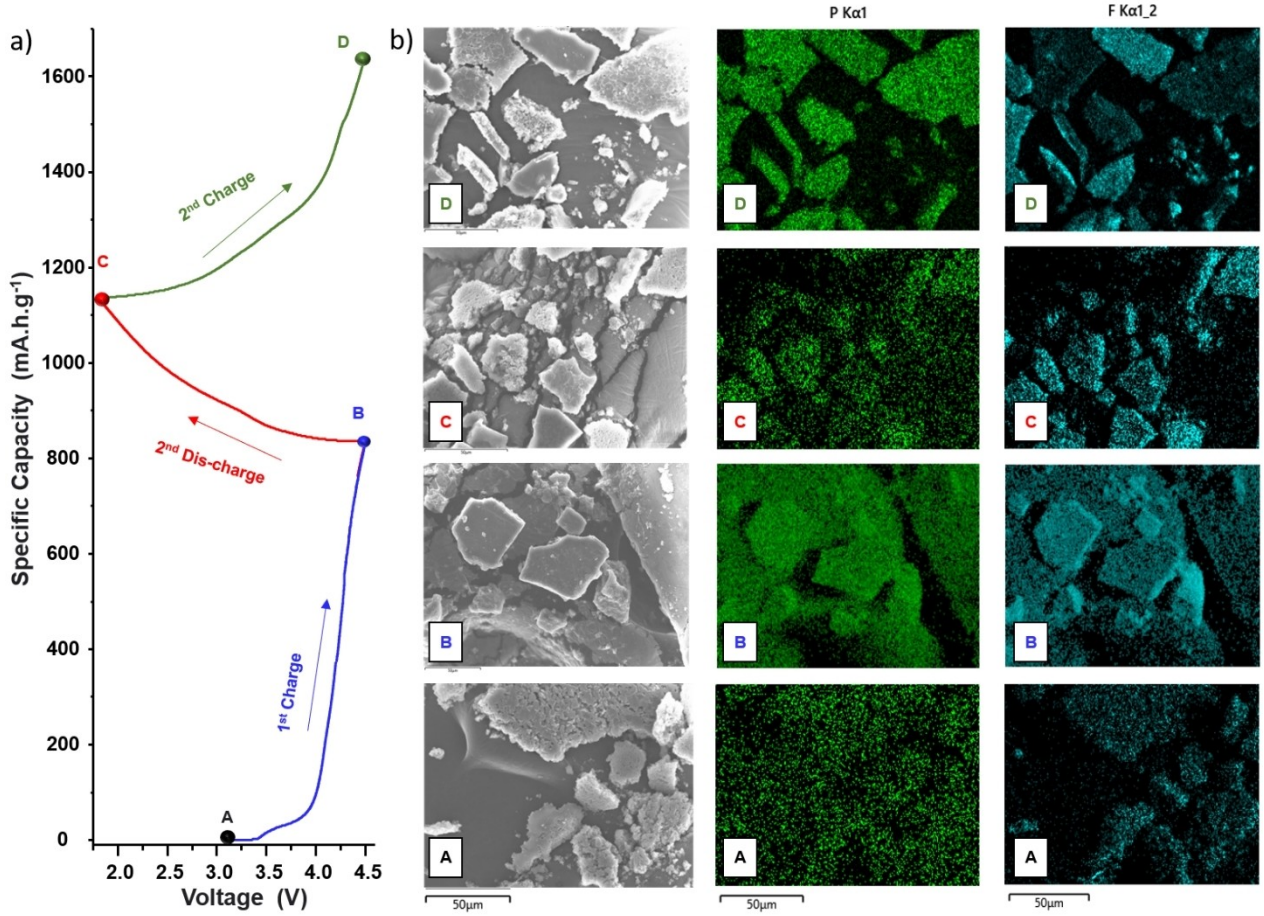

Figure 5. (a) Galvanostatic charge and discharge profile of the CuDEFcP cathode. (b) Ex-situ elemental mapping of the CuDEFcP cathode in different cycles including as prepared (A-after OCV), charged to 4.5 V (B), discharged to 1.8 V (C) and recharged to 4.5 V (D- 2nd cycle).

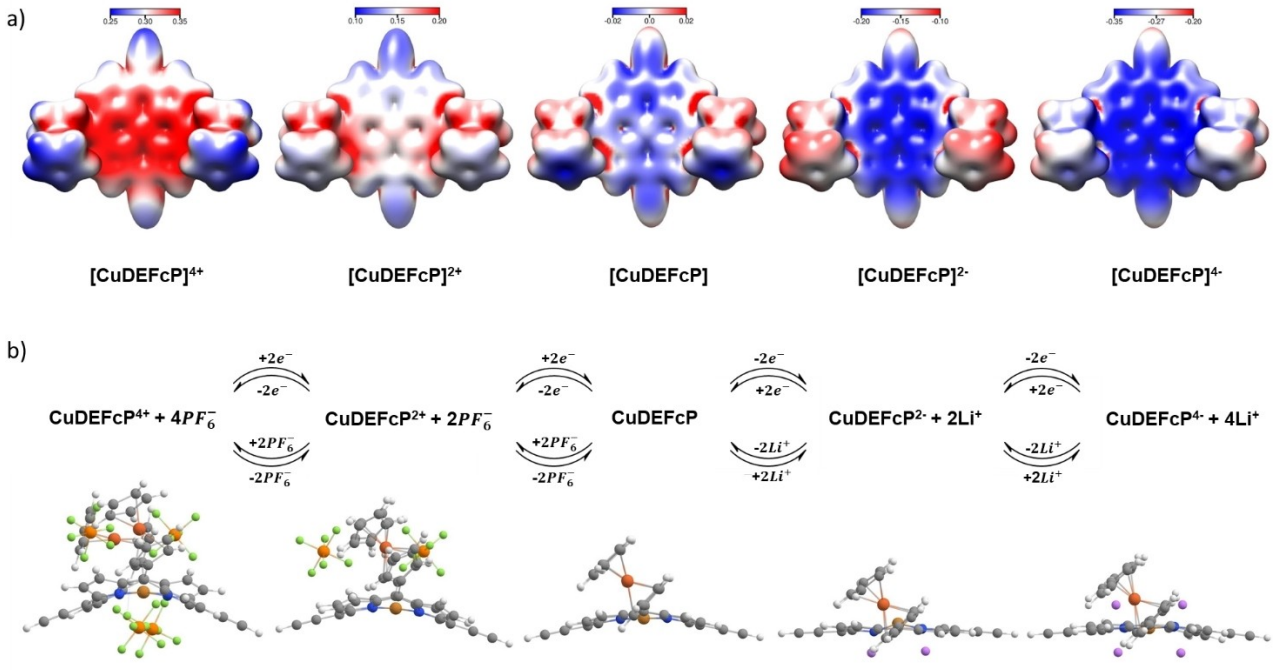

Figure 6. a) Electrostatic potential (ESP) of CuDEFcP in different redox states. b) Spatial structure of $CuDEFcP^{4-} + 4Li^{+}$ (*right*)and $CuDEFcP^{4+} + 4PF_6^-$ (*left*).

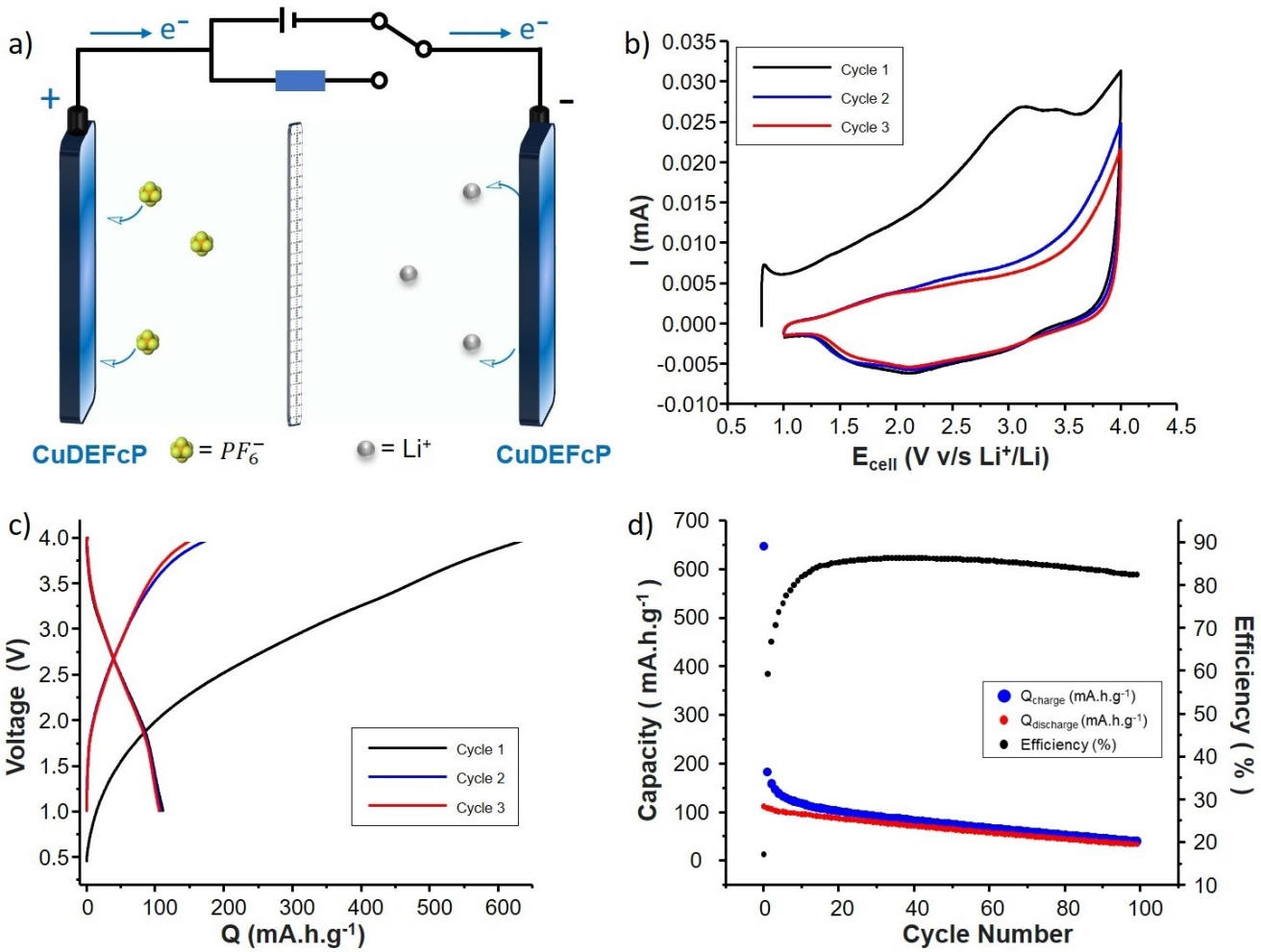

Figure 7. (a) Scheme of SDIBs with CuDEFcP as negative and positive electrode material. b) CV in the range of 1–4 V at a scan rate of 0.1 mV.s^{-1}. (c) Charge and discharge profiles at 100 mA.g^{-1}. (d) Cycling performance at 100 mA.g^{-1}.

473 cm^{-1}[30] broadened and C=N absorption signal shifted from 1501 to 1480 cm^{-1}. These changes indicate that the PF_6^- interacts with the ferrocene and the porphyrin ring (Figure S41). Whereas upon discharging, the signals corresponding to C=N and C–N were less intense than that recorded in the charged state (Figure S41), implying to the interaction of Li^+ with the porphyrin in a region close to the N atoms.

Regarding the irreversible process, as mentioned earlier that the appearance of irreversible oxidation wave at high potential during the first cycle is a common feature with porphyrins.[15a,31] It is independent to the presence or absence of the metal center,[22a] of the nature of the substituents at the porphyrin *meso*-position[14a,15,32] and the type of different metal-based battery system used.[22b,33] Hence as expected, irreversible oxidation waves at a high potential were observed for all of the investigated systems (H_2FcPh_3P, H_2TFcP, CuTFcP and CuDEFcP) during the first charging process (Figure S30 and S42). However, with porphyrins substituted with an ethynyl group, one of the interpretation that has been previously demonstrated using spectroscopic and tomographic techniques is the self-conditioning process which involves the in situ electro-polymerization of ethylene units into the double bonds.[14b] Concerning CuDEFcP featuring an ethynyl moiety, analysis of the cycled electrode revealed the absence of the vibration band of C≡C–H around 3200 cm^{-1} in the IR spectra (Figure S39) along with the formation of interconnected surfaces as observed by SEM (Figure S43) indicated the occurrence of the activation process involving the ethynyl group during the initial charging process which is most likely associated with the self-conditioning process. An additional feature of this interpretation of the observed irreversible oxidation peak could be added that it involves the distortion of the porphyrins structure upon the interaction with PF_6^- ions imposed by its large ionic size as revealed by DFT simulation (Figure S27 and S28). This is further supported by incomplete release of PF_6^- ions during the discharge as revealed by the EDX spectra and the corresponding elemental mapping (Figure 5 and S38).

CuDEFcP as Anode and Cathode Material in a Dual-Ion Organic Symmetric Battery

As stated earlier, porphyrins belong to the bipolar type of organic electrode material. To confirm the bipolar feature of CuDEFcP, it has been utilized as an anode material for LIBs and it displayed good Li^+ storage properties with a high reversible capacity of 295 mAh.g^{-1} (Figure S44–S47). Following that a Dual-Ion Organic Symmetric Battery (SDIBs) has been constructed to fully illustrate the bipolar nature of CuDEFcP, in which the CuDEFcP electrode has been employed as both anode and cathode (Figure 7a).

The electrochemical properties were first evaluated through CV curves, which almost coincide after the first cycle with no well-defined voltage peaks, indicating of multiple redox reactions and good electrochemical stability (Figure 7b). Consistent with the CV profile, the charge/discharge curves showed a highly reversible process after the initial cycle with a slopping voltage plateau around 2.4 V (Figure 7c). The cell delivered a specific discharge capacity of 108 mAh.g^{-1} in the 2nd cycle at a current density of 0.1 A.g^{-1}, corresponding to a specific energy density of 261 Wh.Kg^{-1} and specific power of 188 W.Kg^{-1}. After 100 cycles, the cell maintained a capacity of 35 mAh.g^{-1} with coulombic efficiency of 82.5 % (Figure 7d). In addition, reversible capacities of 80, 74, 68 and 63 mAh.g^{-1} were delivered at current densities of 0.2, 0.3, 0.4 and 0.5 A.g^{-1}, respectively. When the current returned to 0.3 A.g^{-1}, the specific capacity of 63 mAh.g^{-1} was recovered (Figure S48).

Conclusions

In summary, a *bis*-ferrocenyl and *bis*-ethynyl functionalized porphyrin (CuDEFcP) has been developed for the purpose of portraying its bipolar reactivity as electrode material. The presence of electroactive ferrocene units enhanced the capacitive performance when used as cathode material in LIBs. It delivered a high initial capacity of 300 mAh.g^{-1} at 200 mA.g^{-1} and a moderate reversible capacity of 58 mAh.g^{-1} after 5000 cycles at 1 A.g^{-1}. As anode material in LIBs, it delivered a high reversible capacity of 295 mAh.g^{-1}, and can be operated more than 500 times at 200 mA.g^{-1} with good capacity retention. In a symmetric full cell, in which CuDEFcP was deployed as both anode and cathode electrode, the cell delivered an initial capacity of 106 mAh.g^{-1}, with a specific energy of 261 Wh.kg^{-1} and a specific power of 188 W.kg^{-1}. The observed 8-electron transfer process will be used in future for the development of customizable organic electrode materials for energy storage systems, offering novel opportunities for molecular design advancements.

Acknowledgements

This work contributes to the research performed at CELEST (Center for Electrochemical Energy Storage Ulm-Karlsruhe) and was funded by the German Research Foundation (DFG) under Project ID 390874152 (POLiS Cluster of Excellence). Calculations were carried out on the JUSTUS compute cluster. SC wishes to thank the Foundation Jean-Marie Lehn project "QBIRAD" for the financial funding. The authors gratefully acknowledge Dr. Liping Wang for helping in TGA experiment. Open Access funding enabled and organized by Projekt DEAL.

Conflict of Interests

The authors declare no conflict of interest.

Data Availability Statement

The data that support the findings of this study are openly available in Zenodo at 10.5281/zenodo.10390484, reference number 10390484.

Keywords: Organic batteries · Porphyrin · Ferrocene · symmetric cell

[1] R. Huggins, *Advanced batteries: materials science aspects*, Springer Science & Business Media **2008**.
[2] V. Etacheri, R. Marom, R. Elazari, G. Salitra, D. Aurbach, *Energy Environ. Sci.* **2011**, *4*, 3243–3262.
[3] a) M. S. Whittingham, *Chem. Rev.* **2004**, *104*, 4271–4302; b) J. M. Tarascon, M. Armand, *Nature* **2001**, *414*, 359–367; c) X. Zeng, M. Li, D. Abd El-Hady, W. Alshitari, A. S. Al-Bogami, J. Lu, K. Amine, *Adv. Energy Mater.* **2019**, *9*, 1900161.
[4] a) T. B. Schon, B. T. McAllister, P.-F. Li, D. S. Seferos, *Chem. Soc. Rev.* **2016**, *45*, 6345–6404; b) P. Poizot, J. Gaubicher, S. Renault, L. Dubois, Y. Liang, Y. Yao, *Chem. Rev.* **2020**, *120*, 6490–6557.
[5] a) Y. Liang, Y. Yao, *Joule* **2018**, *2*, 1690–1706; b) S. Subhadarshini, N. C. Das, in *Conjugated Polymers for Next-Generation Applications, Vol. 2* (Eds.: V. Kumar, K. Sharma, R. Sehgal, S. Kalia), Woodhead Publishing **2022**, pp. 115–144.
[6] Z. Song, H. Zhou, *Energy Environ. Sci.* **2013**, *6*, 2280–2301.
[7] a) H. Kye, Y. Kang, D. Jang, J. E. Kwon, B.-G. Kim, *Advanced Energy and Sustainability Research* **2022**, *3*, 2200030; b) J. Heiska, M. Nisula, M. Karppinen, *J. Mater. Chem. A* **2019**, *7*, 18735–18758.
[8] a) T. Kakui, S. Sugawara, Y. Hirata, S. Kojima, Y. Yamamoto, *Chem. Eur. J.* **2011**, *17*, 7768–7771; b) C. Liu, D.-M. Shen, Q.-Y. Chen, *J. Am. Chem. Soc.* **2007**, *129*, 5814–5815; c) Y. Yamamoto, A. Yamamoto, S.-y. Furuta, M. Horie, M. Kodama, W. Sato, K.-y. Akiba, S. Tsuzuki, T. Uchimaru, D. Hashizume, F. Iwasaki, *J. Am. Chem. Soc.* **2005**, *127*, 14540–14541; d) S. Chowdhury, Y. Nassar, L. Guy, D. Frath, F. Chevallier, E. Dumont, A. P. Ramos, G. J.-F. Demets, C. Bucher, *Electrochim. Acta* **2019**, *316*, 79–92; e) S. Chowdhury, P. Hennequin, O. Cala, S. Denis-Quanquin, É. Saint-Aman, D. Frath, F. Chevallier, C. Bucher, *J. Porphyrins Phthalocyanines* **2023**, *27*, 1475–1488; f) H.-g. Wang, Q. Wu, L. Cheng, L. Chen, M. Li, G. Zhu, *Energy Storage Mater.* **2022**, *52*, 495–513.
[9] M.-S. Liao, S. Scheiner, *J. Chem. Phys.* **2002**, *117*, 205–219.
[10] H. Wu, J. Zhang, X. Du, M. Zhang, J. Yang, J. Zhang, T. Luo, H. Liu, H. Xu, G. Cui, *Chem. Commun.* **2019**, *55*, 11370–11373.
[11] J.-Y. Shin, T. Yamada, H. Yoshikawa, K. Awaga, H. Shinokubo, *Angew. Chem. Int. Ed.* **2014**, *53*, 3096–3101.
[12] a) K. Tamura, N. Akutagawa, M. Satoh, J. Wada, T. Masuda, *Macromol. Rapid Commun.* **2008**, *29*, 1944–1949; b) Z. Zhao-Karger, P. Gao, T. Ebert, S. Klyatskaya, Z. Chen, M. Ruben, M. Fichtner, *Adv. Mater.* **2019**, *31*, 1806599; c) J. Yuan, B. Ren, X. Feng, P. Gao, E. Liu, S. Tan, *Chem. Commun.* **2020**, *56*, 5437–5440; d) H. Yang, S. Zhang, L. Han, Z. Zhang, Z. Xue, J. Gao, Y. Li, C. Huang, Y. Yi, H. Liu, Y. Li, *ACS Appl. Mater. Interfaces* **2016**, *8*, 5366–5375.
[13] a) H.-g. Wang, H. Wang, Z. Si, Q. Li, Q. Wu, Q. Shao, L. Wu, Y. Liu, Y. Wang, S. Song, H. Zhang, *Angew. Chem. Int. Ed.* **2019**, *58*, 10204–10208;

b) T. Smok, E. Abouzari-Lotf, S. Frentzen, T. Diemant, M. Fichtner, *Batteries & Supercaps* **2023**, *6*, e202300026.
[14] a) P. Gao, Z. Chen, Z. Zhao-Karger, J. E. Mueller, C. Jung, S. Klyatskaya, T. Diemant, O. Fuhr, T. Jacob, R. J. Behm, M. Ruben, M. Fichtner, *Angew. Chem. Int. Ed.* **2017**, *56*, 10341–10346; b) T. Philipp, G. Neusser, E. Abouzari-Lotf, S. Shakouri, F. D. H. Wilke, M. Fichtner, M. Ruben, M. Mundszinger, J. Biskupek, U. Kaiser, P. Scheitenberger, M. Lindén, C. Kranz, *J. Power Sources* **2022**, *522*, 231002; c) X.-M. Lin, D.-Y. Wu, P. Gao, Z. Chen, M. Ruben, M. Fichtner, *Chem. Mater.* **2019**, *31*, 3239–3247; d) H.-g. Wang, Y. Wang, Q. Wu, G. Zhu, *Mater. Today* **2022**, *52*, 269–298.
[15] a) Y. Zhou, X. Huang, X. Chen, F. He, D. Chen, X. Sun, S. Tan, P. Gao, *ACS Appl. Mater. Interfaces* **2022**, *14*, 40862–40870; b) X. Wu, X. Feng, J. Yuan, X. Yang, H. Shu, C. Yang, Z. liu, J. Peng, E. Liu, S. Tan, P. Gao, *Energy Storage Mater.* **2022**, *46*, 252–258.
[16] a) V. N. Nemykin, G. T. Rohde, C. D. Barrett, R. G. Hadt, J. R. Sabin, G. Reina, P. Galloni, B. Floris, *Inorg. Chem.* **2010**, *49*, 7497–7509; b) S. Venkatraman, V. Prabhuraja, R. Mishra, R. Kumar, T. K. Chandrashekar, W. Teng, K. R. Senge, *Indian J. Chem. Sect. A* **2003**, *42*, 2191–2197; c) C. Bucher, C. H. Devillers, J.-C. Moutet, G. Royal, E. Saint-Aman, *Chem. Commun.* **2003**, 888–889; d) P.-O. Schwartz, S. Förtsch, E. Mena-Osteritz, D. Weirather-Köstner, M. Wachtler, P. Bäuerle, *RSC Adv.* **2018**, *8*, 14193–14200.
[17] J. Xie, W. Chen, G. Long, W. Gao, Z. J. Xu, M. Liu, Q. Zhang, *J. Mater. Chem. A* **2018**, *6*, 12985–12991.
[18] Z. Song, H. Zhan, Y. Zhou, *Angew. Chem. Int. Ed.* **2010**, *49*, 8444–8448.
[19] a) F. Ye, Q. Liu, H. Dong, K. Guan, Z. Chen, N. Ju, L. Hu, *Angew. Chem. Int. Ed.* **2022**, *61*, e202214244; b) R. R. Kapaev, A. Zhugayevych, S. V. Ryazantsev, D. A. Aksyonov, D. Novichkov, P. I. Matveev, K. J. Stevenson, *Chem. Sci.* **2022**, *13*, 8161–8170.
[20] Y. Sun, F. He, X. Huang, B. Ren, J. Peng, D. Chen, X. Hu, X. Sun, P. Gao, *Chem. Eng. J.* **2023**, *451*, 138734.
[21] C. Li, C. Zhang, J. Xie, K. Wang, J. Li, Q. Zhang, *Chem. Eng. J.* **2021**, *404*, 126463.
[22] a) S. Shakouri, E. Abouzari-Lotf, J. Chen, T. Diemant, S. Klyatskaya, F. D. Pammer, A. Mizuno, M. Fichtner, M. Ruben, *ChemSusChem* **2023**, *16*, e202202090; b) E. Abouzari-Lotf, R. Azmi, Z. Li, S. Shakouri, Z. Chen, Z. Zhao-Karger, S. Klyatskaya, J. Maibach, M. Ruben, M. Fichtner, *ChemSusChem* **2021**, *14*, 1840–1846.
[23] J. Liu, J. Wang, C. Xu, H. Jiang, C. Li, L. Zhang, J. Lin, Z. X. Shen, *Adv. Sci.* **2018**, *5*, 1700322.
[24] G. Desmaizieres, V. Perner, D. Wassy, M. Kolek, P. Bieker, M. Winter, B. Esser, *Batteries & Supercaps* **2023**, *6*, e202200464.
[25] a) J. C. Bachman, R. Kavian, D. J. Graham, D. Y. Kim, S. Noda, D. G. Nocera, Y. Shao-Horn, S. W. Lee, *Nat. Commun.* **2015**, *6*, 7040; b) T. Liu, K. C. Kim, B. Lee, Z. Chen, S. Noda, S. S. Jang, S. W. Lee, *Energy Environ. Sci.* **2017**, *10*, 205–215.
[26] H.-S. Kim, J. B. Cook, H. Lin, Jesse S. Ko, Sarah H. Tolbert, V. Ozolins, B. Dunn, *Nat. Mater.* **2017**, *16*, 454–460.
[27] K. Sakaushi, G. Nickerl, F. M. Wisser, D. Nishio-Hamane, E. Hosono, H. Zhou, S. Kaskel, J. Eckert, *Angew. Chem. Int. Ed.* **2012**, *51*, 7850–7854.
[28] Y. Lu, X. Hou, L. Miao, L. Li, R. Shi, L. Liu, J. Chen, *Angew. Chem. Int. Ed.* **2019**, *58*, 7020–7024.
[29] a) L. Liu, L. Miao, L. Li, F. Li, Y. Lu, Z. Shang, J. Chen, *J. Phys. Chem. Lett.* **2018**, *9*, 3573–3579; b) H.-G. Wang, H. Wang, Y. Li, Y. Wang, Z. Si, *J. Energy Chem.* **2021**, *58*, 9–16.
[30] S. Radhakrishnan, S. Paul, *Sens. Actuators B* **2007**, *125*, 60–65.
[31] a) X. Chen, X. Feng, B. Ren, L. Jiang, H. Shu, X. Yang, Z. Chen, X. Sun, E. Liu, P. Gao, *Nano-Micro Lett.* **2021**, *13*, 71; b) Z. Chen, P. Gao, W. Wang, S. Klyatskaya, Z. Zhao-Karger, D. Wang, C. Kübel, O. Fuhr, M. Fichtner, M. Ruben, *ChemSusChem* **2019**, *12*, 3737–3741.
[32] F. He, Y. Zhou, X. Chen, T. Wang, Y. Zeng, J. Zhang, Z. Chen, W. Liu, P. Gao, *Chem. Commun.* **2023**, *59*, 2787–2790.
[33] S. Lv, J. Yuan, Z. Chen, P. Gao, H. Shu, X. Yang, E. Liu, S. Tan, M. Ruben, Z. Zhao-Karger, M. Fichtner, *ChemSusChem* **2020**, *13*, 2286–2294.

Manuscript received: December 18, 2023
Revised manuscript received: January 15, 2024
Accepted manuscript online: January 24, 2024
Version of record online: ■■, ■■

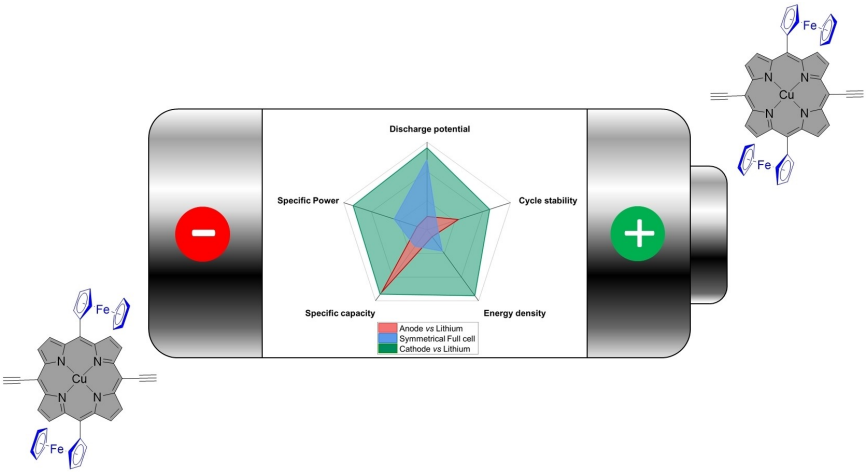

S. Chowdhury, S. Jana, S. P. K. Panguluri, W. Wenzel, S. Klayatskaya*, M. Ruben**

1 – 10

Ferrocene Appended Porphyrin-Based Bipolar Electrode Material for High-Performance Energy Storage

The flexible, sustainable, and environmentally friendly nature of bipolar redox organics has generated significant interest in their utilization as electrode materials for energy storage. In this perspective, a novel copper(II)[5,15-bis(ethynyl)-10,20-di ferrocenyl porphinato] – (CuDEFcP) has been developed and employed as electrodes in rechargeable energy-storage systems. As a cathode material in LIBs, it delivered a high initial discharge capacity of 300 mAh.g^{-1} at 200 mA.g^{-1} and a moderate reversible capacity of 58 mAh.g^{-1} after 5000 cycles at 1 A.g^{-1}. Whereas when CuDEFcP employed as anode material in LIBs, a reversible capacity of 295 mAh.g^{-1} was delivered at 200 mA.g^{-1}. In a symmetric full cell, a specific energy of 261 Wh.kg^{-1} and a specific power of 188 W.kg^{-1} was obtained.